ADVANCED MATERIALS
www.advmat.de

Sphingosine 1-Phosphate Liposomes for Targeted Nitric Oxide Delivery to Mediate Anticancer Effects against Brain Glioma Tumors

Yang Liu, Xiao Wang, Jing Li, Jian Tang, Bin Li, Yu Zhang, Ning Gu, and Fang Yang**

Specifically targeting glioblastoma multiforme (GBM) blood vessels and actively enhancing the permeability of the brain–blood–tumor barrier (BBTB) are two extremely difficult challenges currently hindering the development of effective therapies against GBM. Herein, a liposome drug delivery system (S1P/JS-K/Lipo) is described, which delivers the nitric oxide (NO) prodrug JS-K, O_2-(2,4-dinitrophenyl) 1-[(4-ethoxycarbonyl) piperazin-1-yl] diazen-1-ium-1,2-diolate, to GBM tumors using sphingosine-1-phosphate (S1P)-signaling molecules as active targeting lipid ligands. It is revealed that S1P/JS-K/Lipo actively penetrates the BBTB, aided by caveolin-1-mediated transcytosis, and it is demonstrated that the system specifically interacts with S1P receptors (S1PRs), which are highly expressed on GBM cells. Nondestructive ultrasound imaging in GBM mouse models is also utilized to observe microsized NO bubble production from JS-K, as catalyzed by the glutathione *S*-transferases (GSTs) resident in GBM cells. Given that these NO bubbles strongly promote GBM cell death in vivo, the S1PR-targeted liposome delivery system—which successfully achieves BBTB penetration and tumor targeted delivery of a complex multicomponent drug regimen—represents a promising approach for targeted therapies against GBM and other carcinomas characterized by elevated S1PR expression.

1. Introduction

Glioblastoma multiforme (GBM), a WHO grade IV astrocytoma, accounts for the majority of all gliomas (60–70%).[1,2] It is an invasive primary tumor of the central nervous system (CNS), with less than a 6% five-year survival rate.[3] The current standard of care for GBM is the use of gefitinib, erlotinib, and temozolomide chemotherapeutic drugs.[4–8] However, due to low targeting efficacies and *P*-glycoprotein (*P*-gp) efflux pump related drug-resistance, none of these (nor related modified therapies) have shown statistically robust improvements over placeboes for GBM treatment.[9–11] The major challenges limiting effective drug therapies against GBM include: 1) a lack of demonstrated targets vulnerable to effective intervention; and 2) low therapeutic accumulation levels at tumor sites, owing to the physical and biochemical functions of the blood–brain–tumor barrier (BBTB).[12–14] This BBTB penetration issue is particularly challenging, as nonuniform permeability and active drug efflux from the BBTB microenvironment around cancer cells can strongly hinder drug efficacy effectiveness against primary brain tumors.[15–18]

Nitric oxide (NO) has been reported to play an important role in tumor biology.[19–22] The administration of high concentrations NO has been shown to cause nitrosative stress and subsequently induce cancer cell apoptosis.[23,24] Although this therapy exhibits a strong potential for cancer treatment, the short half-life, low bioavailability, and poor tumor targeting of most NO-delivery agents have, to date, limited in vivo efficacy.[25–27] To overcome these challenges, we have fabricated a liposomal drug delivery system that delivers a NO prodrug (JS-K, O_2-(2,4-dinitrophenyl) 1-[(4-ethoxycarbonyl) piperazin-1-yl] diazen-1-ium-1,2-diolate) to GBM using sphingosine-1-phosphate (S1P)-signaling molecules as active targeting lipid ligands (S1P/JS-K/Lipo). Clinical reports have demonstrated that S1P concentration is significantly elevated in GBM; given the specific high affinity between bioactive lipid S1P signal molecules and the transmembrane G-protein-coupled receptors family of sphingosine-1-phosphate receptors (S1PRs), these signaling molecules have the potential to enable targeted NO therapeutic agent delivery to tumor cells for GBM treatment.[28–31] Based on these extensive data, we selected bioactive S1P molecules as our BBTB receptor target for this proof-of-concept work establishing an in situ GBM targeted drug delivery platform. Further, we selected JS-K NO prodrugs as the theranostic agent to utilize the high concentration of in situ NO production to both induce anticancer effects and provide ultrasound imaging to monitor target engagement. By combining the liposomal drug delivery platform with S1P molecules, we demonstrate that S1P/JS-K/Lipo is capable of generating a specific response to BBTB endothelial cells and enhances targeting efficiency to glioma cells in both a Transwell in vitro system as well as GBM-bearing mice. Furthermore, we elucidate that the

Y. Liu, X. Wang, J. Li, J. Tang, B. Li, Prof. Y. Zhang, Prof. N. Gu, Prof. F. Yang
State Key Laboratory of Bioelectronics
Jiangsu Key Laboratory for Biomaterials and Devices
School of Biological Sciences and Medical Engineering
Southeast University
Nanjing 201196, P. R. China
E-mail: guning@seu.edu.cn; yangfang2080@seu.edu.cn

The ORCID identification number(s) for the author(s) of this article can be found under https://doi.org/10.1002/adma.202101701.

DOI: 10.1002/adma.202101701

BBTB crossing mechanism of S1P/JS-K/Lipo is mediated by Cavelion-1 enhanced endocytosis and *P*-gp efflux inhibition.

2. Results and Discussion

2.1. Fabrication and Characterization of S1P/JS-K/Lipo

An overview of our overall approach to stabilize the reactive NO-releasing agents for facilitating delivery of therapeutic NO doses to glioma region is shown in **Figure 1**. The prodrug JS-K (O_2-(2,4-dinitrophenyl) 1-[(4-ethoxycarbonyl) piperazin-1-yl] diazen-1-ium-1,2-diolate) is a diazeniumdiolate that releases NO after enzymatic metabolization by glutathione *S*-transferases (GSTs), but its clinical use has been limited by its poor water solubility.[32] Thus, we fabricated a liposome formulation (S1P/JS-K/Lipo), which combines JS-K as NO prodrug with S1P as targeting molecules in the lipid shell. To provide analogous controls, control liposome without the JS-K or S1P components (Lipo) and liposomes encapsulated

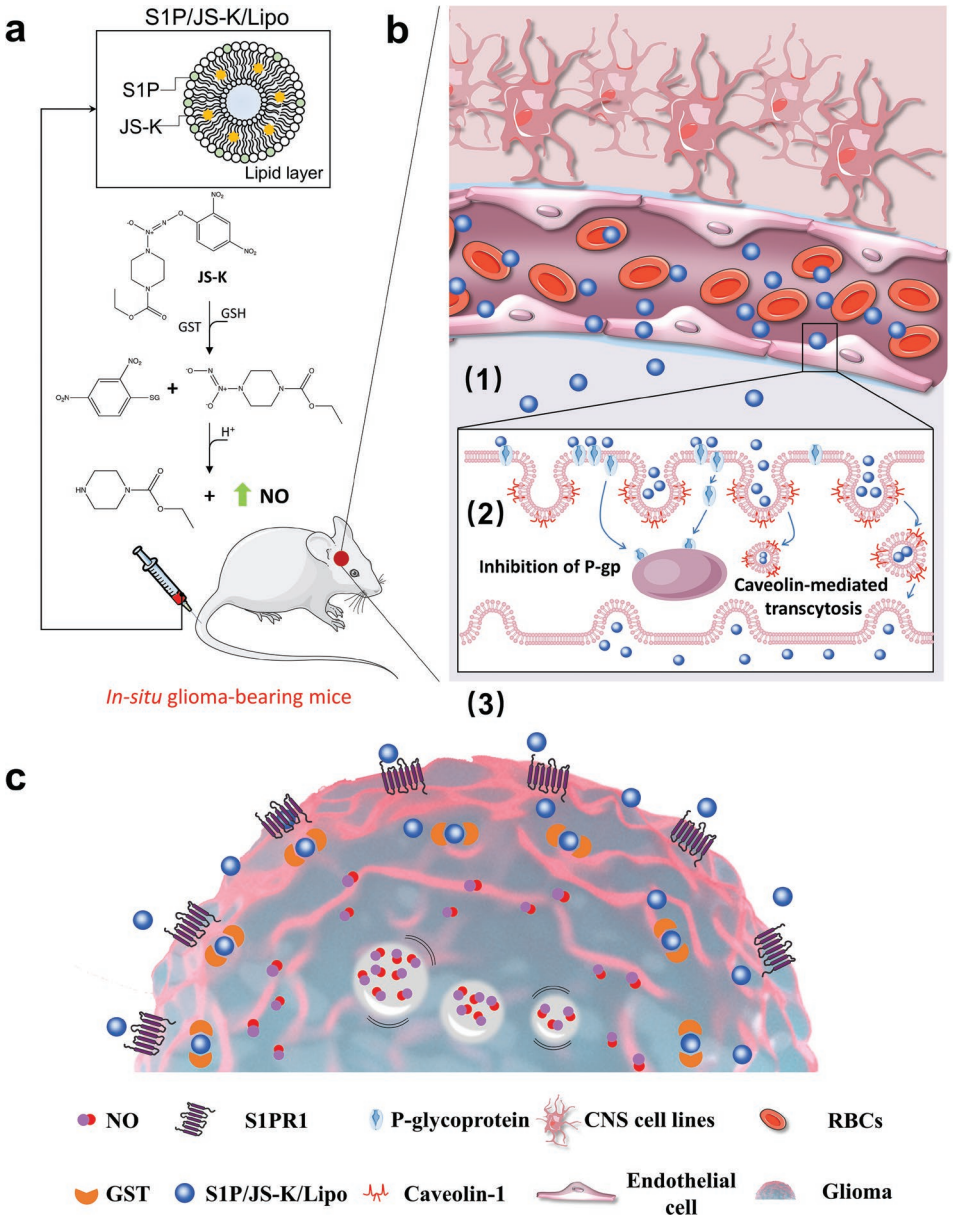

Figure 1. Design features and proposed mechanism of action of S1P/JS-K liposome targeting of brain glioma tumors. a) Schematic illustration of the preparation of S1P/JS-K/Lipo. S1P, sphingosine-1-phosphate; JS-K, (O_2-(2, 4- dinitrophenyl) 1-[(4- ethoxycarbonyl) piperazin-1-yl] diazen-1-ium-1,2-diolate), organic nitric oxide (NO) donors. b) Schematic indicating the anticipated sequential targeting of S1P/JS-K/Lipo to the BBTB and to brain glioma tumors in mice: 1) S1P/JS-K/Lipo encounters the surface of tumor endothelial cells based on the specific S1P interaction with S1PRs on the endothelial cells, S1P/JS-K/Lipo accumulates at the glioma tumor region; 2) S1P/JS-K/Lipo transmigrates across the BBTB via caveolae-mediated transendothelial transcytosis with inhibition the *P*-glycoprotein (*P*-gp); 3) S1P/JS-K/Lipo penetrates glioma tumor cells. c) Schematic showing that S1P/Lipo/Lipo is activated by concentrated GST enzymes and releases JS-K molecules in the tumor microenvironment, resulting in the continuous generation of microsized NO bubbles and producing an antitumor effect. Concurrently, NO bubble generation can be imaged via real-time ultrasound imaging.

with only S1P (S1P/Lipo) and JS-K (JS-K/Lipo) were also constructed.

Transmission electron microscopy (TEM) demonstrated that S1P/JS-K/Lipo appeared as well-dispersed spherical structures (**Figure 2**a). The average hydrodynamic diameter of liposomes increased from 164 to 177 nm upon loading with JS-K. Further modification by the S1P targeting molecules resulted in an additional increase in diameter to 189 nm for S1P/JS-K/Lipo (Figure 2b; Table S1, Supporting Information). The hydrodynamic diameter and zeta potential of S1P/JS-K/Lipo showed no significant change with testing for up to 20 days storage in PBS at pH 7.4 (Figure 2c), exhibiting the excellent stability of S1P/JS-K/Lipo. Once the fluorescent dye DiR was incorporated into liposomes with JS-K, or when fluorescein isothiocyanate (FITC) was covalently linked to S1P molecules in S1P/JS-K/Lipo, the fluorescence of the labeled liposomes remained largely unchanged for 24 h, suggesting that S1P and JS-K are stably encapsulated within the liposome (Figure S1, Supporting Information). Figure 2d shows the different Fourier transform infrared (FT-IR) rapid-scan spectrum of S1P,

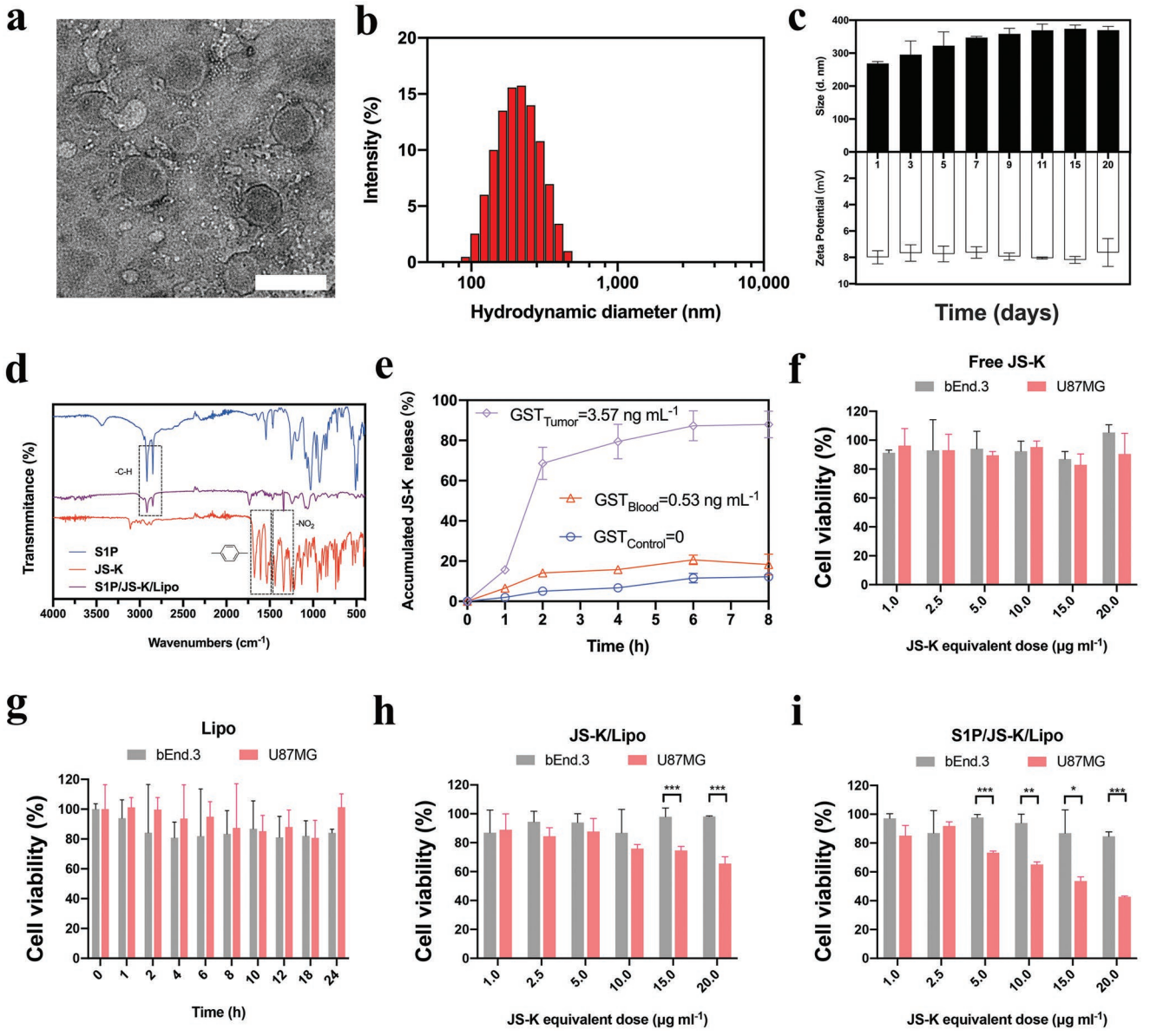

Figure 2. Preparation, characterization, and cell cytotoxicity of S1P/JS-K/Lipo. a) Transmission electron microscopy (TEM) morphology characterization of S1P/JS-K/Lipo. Scale bar: 100 nm. b) Histogram of particle-size distribution of S1P/JS-K/Lipo obtained by DLS measurements. c) The in vitro stability of S1P/JS-K/Lipo in PBS (pH = 7.4) at 1, 3, 5, 7, 9, 11, 15, and 20 days, measured by DLS, and the zeta potential under physiological pH conditions. Error bars: mean ± standard deviation (SD) ($n = 3$). d) FT-IR scanning of lyophilized powder of free JS-K, S1P, and S1P/JS-K/Lipo. e) JS-K released from S1P/JS-K/Lipo in saline solution with GSH (200 mg L^{-1}) under different GST concentrations ($GST_{Control} = 0$, $GST_{Blood} = 0.53$ ng mL^{-1}, and $GST_{Tumor} = 3.57$ ng mL^{-1}). Error bars: mean ± SD ($n = 3$). f–i) Cytotoxicity of free JS-K, Lipo, JS-K/Lipo, and S1P/JS-K/Lipo for both bEnd.3 cells and U87MG cells. The cells were incubated with the liposome formulations for 24 h. Error bars: mean ± SD ($n = 3$). $^{*}P < 0.05$, $^{**}P < 0.01$, and $^{***}P < 0.001$, in comparison between bEnd.3 cells and U87MG cells using an unpaired Student's *t*-test (two-tailed).

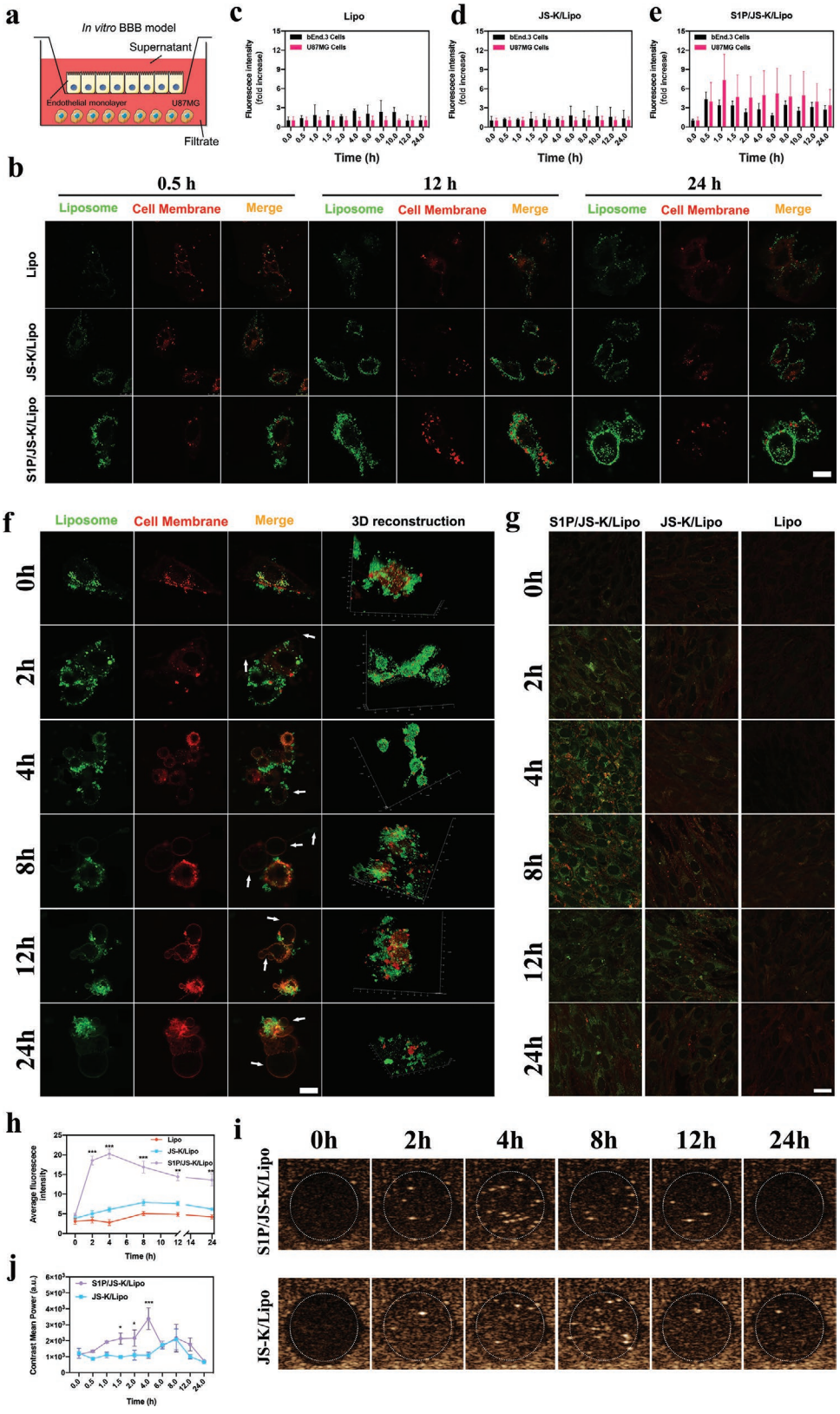

Figure 3. In vitro penetration of S1P/JS-K/Lipo across the BBTB. a) Schematic illustration of the classic Transwell system based in vitro BBTB for evaluating the penetration capability of S1P/JS-K/Lipo across the endothelial monolayer. b) Confocal laser scanning microscopy (CLSM) images of colocalization of bEnd.3 cells after co-incubation with Lipo, JS-K/Lipo, or S1P-FITC/JS-K/Lipo over time. The cell membrane of bEnd.3 cells was stained with DiI, and the shell of liposome formulations was stained with green fluorescence. The merge images are the overlay of the two individual images.

JS-K, and S1P/JS-K/Lipo formulation. The stretch signal at 2950–2850 cm^{-1} of alkyl groups in the free S1P appear in S1P/JS-K/Lipo. Both the N–O stretch signal at 1360–1290 cm^{-1} of nitro-aromatic groups and C–C stretch signal at 1610–1370 cm^{-1} of aromatic ring in JS-K also appear in S1P/JS-K/Lipo. These results demonstrate that the S1P and JS-K molecules were successfully combined with the lipid bilayer of S1P/JS-K/Lipo formulation.

2.2. JS-K Release from S1P/JS-K/Lipo Is Determined by GST Concentrations

The stability and release profiles for the enzyme-catalyzed transformation of JS-K in S1P/JS-K/Lipo were evaluated under different GST concentrations with high-performance liquid chromatography (HPLC). The tested GST concentrations for simulating the liposome interaction were 0, 0.53, and 3.57 ng mL^{-1}, respectively, under conditions mimicking normal storage buffers, "GST_{Blood}:" representing a typical peripheral blood concentration GST,[33] and "GST_{Tumor}:" representing a typical tumor concentration.[34] The liposome lipid layer inhibits the explosive release and diffusion of JS-K from S1P/JS-K/Lipo under normal, without GSH, and GST storage conditions: only a 12% release of JS-K was observed in solution within the 8 h testing window (Figure 2e). Similarly, <20% JS-K leakage from the S1P/JS-K/Lipo formulation occurred in GSH (200 mg L^{-1}) solution under GST_{Blood} treatment. In stark contrast, S1P/JS-K/Lipo exhibited significantly enhanced JS-K release in GSH (200 mg L^{-1}) solution under GST_{Tumor} concentration, which mimics the known concentration of GST in glioma tumor microenvironments: a 50% burst release of JS-K occurred within the first 2 h, and the total drug release over 8 h reached >90%. Collectively, these data suggest that S1P/JS-K/Lipo can preserve stability during circulation process but can rapidly release JS-K in the presence of GST concentrations typical in GBM tumors.

2.3. Cytotoxicity of S1P/JS-K/Lipo

Brain microvascular endothelial (bEnd.3) cells and glioma tumor (U87MG) cells were used to assess cytotoxicity upon interaction with free JS-K, control Lipo, JS-K/Lipo, or S1P/JS-K/Lipo. Cell cytotoxicity was determined via Cell Counting Kit-8 cell (CCK-8) proliferation assay under differing JS-K concentrations (1.0, 2.5, 5.0, 10.0, 15.0, and 20.0 μg mL^{-1}) for 24 h (Figure 2f–i). The free JS-K, JS-K/Lipo, and S1P/JS-K/Lipo treatments at concentrations <20 μg mL^{-1} had negligible effects on bEnd.3 cell viability. However, JS-K/Lipo exhibited enhanced cytotoxicity against U87MG cells, with the IC50 of JS-K/Lipo against U87MG cells at 34.3 μg mL^{-1} (JS-K equivalent) compared to 55.5 μg mL^{-1} for the free JS-K, suggesting that the liposome formulation facilitated the cellular uptake of the therapeutic agent. Once the JS-K/Lipo were modified with the targeting S1P molecule on the lipid shell, the IC50 values of S1P/JS-K/Lipo on U87MG cells significantly decreased (16.5 μg mL^{-1}), suggesting that S1P effectively triggers the intracellular uptake of liposomes by U87MG cells.

2.4. S1P-Mediated Active BBTB Penetration Enhancement of S1P/JS-K/Lipo

We next assessed how the S1P molecules function in promoting the intercellular trafficking of S1P/JS-K/Lipo from endothelial cells to tumor cells (i.e., across the BBTB). These experiments were based on a well-established Transwell system, comprising a monolayer of brain microvascular endothelial (bEnd.3) cells in the top well and glioma tumor (U87MG) cells in the bottom well for in vitro assessment of the BBTB penetration capability of S1P/JS-K/Lipo (**Figure 3**a; Figure S2, Supporting Information). Liposome shells of different formulations were stained with green fluorescent dyes, and the cell membranes of bEnd.3 cells were stained with red fluorescent dyes (1,1′-dioctadecyl-3,3,3′,3′-tetramethylindocarbocyanine perchlorate, DiI). As shown in Figure 3b, compared with the Lipo and JS-K/Lipo formulation, the S1P-FITC/JS-K/Lipo formulation exhibits higher permeability through the monolayer. The median fluorescence intensity of U87MG cells treated with Lipo and JS-K/Lipo in the bottom well for 24 h showed only 1.01- and 1.05-fold enhancement, respectively, compared to those at 0 h (Figures S3–S5, Supporting Information).

In contrast, the median fluorescence intensity of bEnd.3 cells treated with S1P/JS-K/Lipo in the upper well dramatically increased (2.71-fold enhancement), showing rapid accumulation (≈0.5 h); further, a nearly 3.38-fold enhancement in median fluorescence intensity occurred in U87MG cells in the bottom well (Figure 3b–e). With an increase in incubation time, a corresponding decrease in the median fluorescence intensity occurred in the bEnd.3 cells, and this was accompanied by an increase in intensity in the U87MG cells of the bottom well. These results highlight that S1P/JS-K/Lipo can penetrate efficiently across the BBTB and enter into the glioma brain region.

Scale bar, 25 μm. c–e) Quantitative change in fluorescence intensities of liposomes in both bEnd.3 cells and U87MG cells co-incubated with Lipo, JS-K/Lipo, and S1P/JS-K/Lipo. Data are shown as mean ± SD ($n = 3$ independent experiments). Error bars: mean ± SD ($n = 3$). f) CLSM image of U87MG cells treated with S1P/JS-K/Lipo at different time points (0, 2, 4, 8, 12, and 24 h). The cell membranes of U87MG cells were stained with DiI, and the shell of S1P-FITC/JS-K/Lipo was stained with green fluorescence. There were sharply contrasting outcomes depending upon different incubation durations: the S1P/JS-K/Lipo-treated DiI-U87MG cells showed a release of JS-K and evident in situ formation of gas bubbles in cell membranes (white arrows). Scale bar = 25 μm. g) Photomicrographs of NO production over time in U87MG cells pretreated with DAF-FM DA, and then incubated with S1P/JS-K/Lipo, JS-K/Lipo, or Lipo for 24 h in 10% FBS medium. Scale bar: 20 μm. h) Quantitative analysis of fluorescence intensity of NO in U87MG cells co-incubated with Lipo, JS-K/Lipo, or S1P/JS-K/Lipo. Error bars: mean ± SD ($n = 3$). $^{**}P < 0.01$ and $^{***}P < 0.001$ in comparison between Lipo, JS-K/Lipo, and S1P/JS-K/Lipo groups using a one-way ANOVA. i) In vitro ultrasound images of U87MG cells in agarose gel phantom after incubation with JS-K/Lipo or S1P/JS-K/Lipo for the indicated times. j) Quantitative contrast mean power of ultrasound images. Error bars: mean ± SD ($n = 3$). $^{*}P < 0.05$ and $^{***}P < 0.001$, in comparison between S1P/JS-K/Lipo and JS-K/Lipo using an unpaired Student's *t*-test (two-tailed).

2.5. S1P-Mediated U87MG Cell Active Targeting and Improved Intracellular Uptake of S1P/JS-K/Lipo

We further evaluated the potential tumor cell targeting and cell killing impacts of S1P/JS-K/Lipo for U87MG cells. We observed that U87MG cells naturally adhered to the bottom surface of the lower well of the Transwell apparatus, exhibiting smooth morphology before treatment (Figure 3f). However, within 2 h of S1P/JS-K/Lipo treatment, the edges of the cells began to become irregular and some small intracellular bubble-like bumps appeared (white arrows in Figure 3f; Figure S6, Supporting Information). After 4 h incubation, the cells were obviously disrupted and had detached from the bottom surface and formed into spherical shapes. After 12 h incubation, 30% of the glioma cells were ruptured, and the remaining 70% of unruptured cells showed bubble-like structures. By 24 h incubation, >95% of the cells were broken into irregular debris.

We next preincubated U87MG cells with the NO-sensitive specific fluorescent labeled probe 4-amino-5-aminomethyl-2′,7′-difluorofluorescein diacetate (DAF-FM DA).[35] After 2 h incubation with S1P/JS-K/Lipo, U87MG cells exhibited stronger NO fluorescence signals compared to cells treated with JS-K/Lipo and Lipo, indicating that S1P facilitates intracellular internalization of the liposomal drug delivery system (Figure 3g). Gradual increases in fluorescence intensity were observed with increasing co-incubation for both the S1P/JS-K/Lipo and JS-K/Lipo groups, but at all time points the fluorescence intensity of the S1P/JS-K/Lipo cells was invariably stronger than the JS-K/Lipo cells until cell rupture) (Figure 3h). Consistent with NO gas causing cell rupture (Figure 3f), the DAF-FM DA probe signal for the S1P-FITC/JS-K/Lipo samples dropped once cell rupturing began around 4 h.

2.6. Intracellular NO Bubble Production with Ultrasound Imaging Monitoring

In order to understand the increased catalytic generation of NO gas in U87MG cells upon the enhanced intracellular uptake of S1P/JS-K/Lipo, ultrasound imaging was used to visualize NO bubble generation. Representative contrast-mode sonograms of the cells incubated with S1P/JS-K/Lipo showed gradually increased echo signals compared to the Lipo control group (Figure 3i; Figure S7, Supporting Information). Indeed, the sonograms showed that the S1P/JS-K/Lipo samples had the largest bubble echo intensity among the tested liposome formulations, with the apparent peak of intracellular NO accumulation occurring at 4 h S1P/JS-K/Lipo treatment (Figure 3j).

2.7. S1P/JS-K/Lipo Promotes BBTB Penetration and Enhanced Tumor Accumulation

The rapid cellular uptake of S1P/JS-K/Lipo by bEnd.3 cells may be due to S1P-mediated transcytosis through the cells comprising the BBTB. To validate whether transcellular transport (transcytosis) facilitates S1P/JS-K/Lipo penetration through the BBTB, we treated bEnd.3 cells with a red fluorescently labeled caveolin-1 antibody after first culturing cells with S1P-FITC/JS-K/Lipo, JS-K/DiO-Lipo, or DiO-Lipo for various time intervals. While the caveolin-1 fluorescence intensity in bEnd.3 cells incubated with DiO-Lipo, JS-K/DiO-Lipo, and S1P-FITC/JS-K/Lipo were negligible within 24 h (**Figure 4**a), the S1P-FITC/JS-K/Lipo group showed significant fluorescence colocalization with caveolin-1 substantially earlier and with significantly enhanced fluorescence intensity, compared to cells incubated with DiO-Lipo or JS-K/DiO-Lipo (Figure S8, Supporting Information).

S1P/JS-K/Lipo gradually colocalized with the caveolin-1 tracker in locally magnified images, in which S1P/JS-K/Lipo and caveolin-1 formed a strikingly regular spherical shape (Figure 4a). Pearson correlation coefficient between red signals (caveolin-1) and green signals (liposome formulations) reached 0.80 after 1 h treatment (Figure 4b–g), indicating that most of the internalized S1P/JS-K/Lipo were transported to the caveolae organelle structures formed by caveolin-1.[9] In contrast, only a few signals of internalized Lipo or JS-K/Lipo were colocalized with the ring structure of caveolae, with maximal Pearson correlation coefficients of 0.01 and 0.14, respectively, upon 12 h incubation. Given that transcytosis is characteristic of a rapid cellular uptake at one side of a cell and exocytosis on the opposite,[36] our results demonstrate that the modified S1P molecules on the liposomes enhance the active uptake capacity of endothelial cells through caveolae-mediated endocytosis; such transport is promoted by the interaction of S1P/JS-K/Lipo with S1PR at the cell membrane and this increases the formation of caveolae.

The transmembrane *P*-glycoprotein efflux pump (*P*-gp) has been shown to pump chemotherapy drugs out of cells;[37–39] S1P is known to decrease *P*-gp expression and membrane levels.[29,40,41] To determine whether *P*-gp efflux capacity is influenced by S1P/JS-K/Lipo endocytosis into bEnd.3 cells, we studied the exocytosis and transcellular transfer of S1P/JS-K/Lipo treatment differing time intervals while tracking *P*-gp via a fluorescently labeled antibody. Given a previous report that increased S1P-S1PR interaction in endothelial cells causes a reduction in *P*-gp levels,[42] we monitored the time-dependent *P*-gp changes in bEnd.3 cells upon treatment with DiO-Lipo or JS-K/DiO-Lipo as compared to untreated control cells at 7 tested time points (0.5, 1, 2, 4, 8, 12, and 24 h). Increased *P*-gp levels resulted in the decreased liposome formulation in cells (Figure 4h). Cells incubated with S1P/JS-K/Lipo exhibited clearly reduced *P*-gp levels and large amounts of the S1P/JS-K/Lipo were observed in these cells. These findings confirm that the S1P-mediated activation of S1PR can repress *P*-gp levels and indicate that this repression may contribute to the strong accumulation of S1P/JS-K/Lipo in bEnd.3 cells and consequently support *P*-gp-mediated exocytosis toward targeted U87MG cells.

2.8. S1P/Lipo/Lipo Can Penetrate the BBTB and Accumulate in Brain Glioma Cancers In Vivo

To assess S1P/JS-K/Lipo function in vivo, we generated tumor implants in mice from human U87MG-RFP cells. At 14 days postimplantation, when the tumor volume had reached 50 mm^3, the mice were randomly divided into five groups ($n = 8$ per group): Group 1, mice model injected with saline; Group 2,

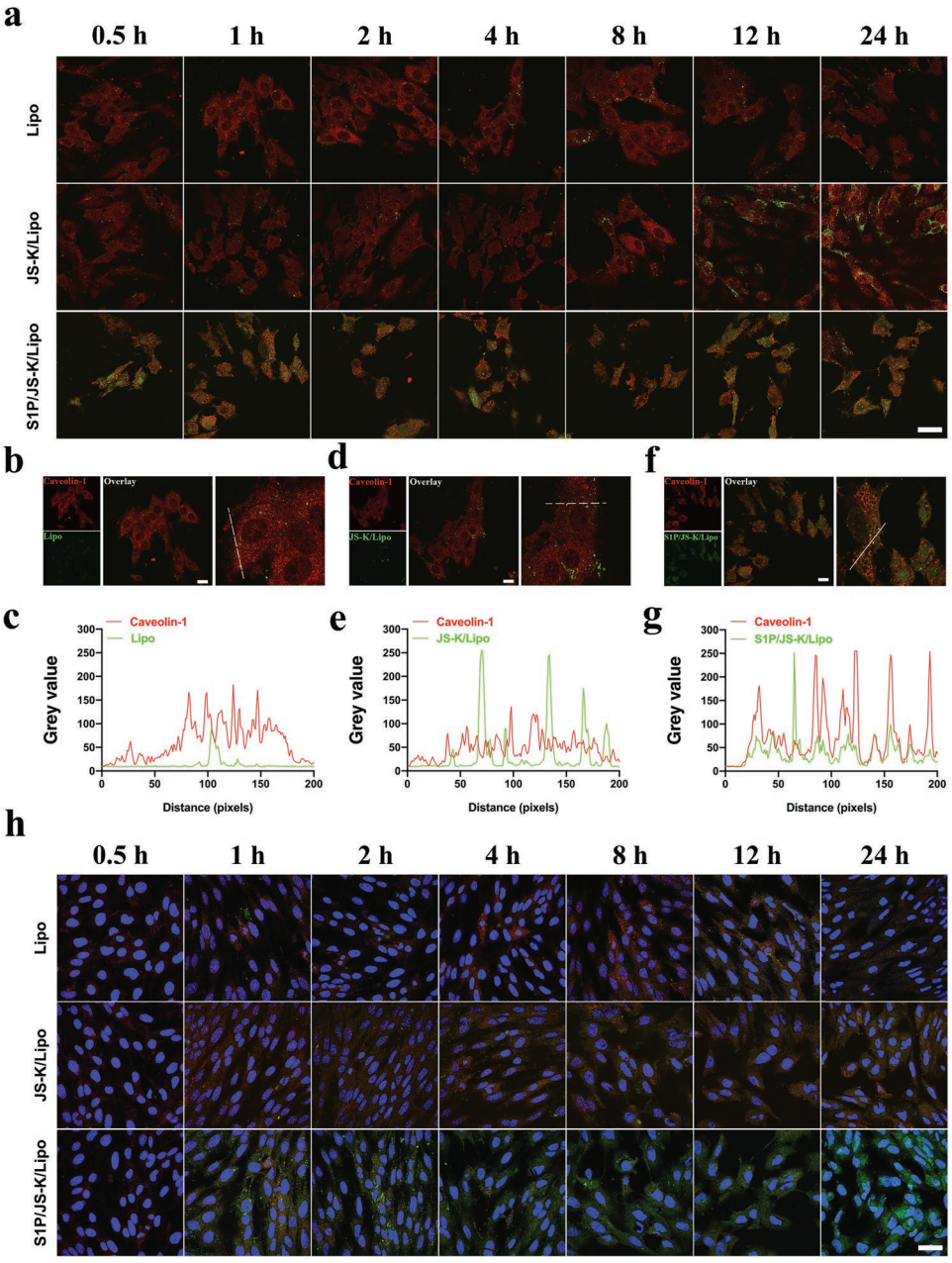

Figure 4. S1P-directed sequential delivery and glioma cell killing. a) CLSM images of caveolin-1 and green fluorescence labeled liposome formulations present in the bEnd.3 cells at the indicated time points. Caveolin-1 was stained with Alexa Fluor 488 conjugated caveolin-1 antibody. Scale bar: 40 µm. b,d,f) CLSM images of colocalization of caveolin-1 with DiO-Lipo (b), JS-K/DiO-Lipo (d), and S1P-FITC/JS-K/Lipo (f) after 1 h culture with bEnd.3 cells. c,e,g) Alexa Fluor 488 red fluorescence and DiO-Lipo (c), JS-K/DiO-Lipo (e), and S1P-FITC/JS-K/Lipo (g). The caveolin-1 and liposome fluorescence intensity profiles across the cell were measured along the selected line (indicated by the white lines in the inset images of (b), (d), and (f)). The fluorescence of caveolin-1 and DiO-Lipo (b), JS-K/DiO-Lipo (d), and S1P-FITC/JS-K/Lipo (f) was calculated by pixel intensity using Image J software. Caveolae fluorescence is red, and the fluorescence of the control liposomes, JS-K/Lipo, and S1P/JS-K/Lipo groups are green. Scale bars: 20 µm. h) The effects of liposome incubation on cell exocytosis and intracellular transfer by *P*-gp, visualized by confocal microscopy. bEnd.3 cells (≈10^5) on confocal dishes were cultured medium containing Lipo, JS-K/Lipo, or S1P/JS-K/Lipo for different durations. Dishes were rinsed and imaged. Scale bars: 40 µm.

mice injected with Lipo; Group 3, mice injected with S1P/Lipo; Group 4, mice injected with JS-K/Lipo; Group 5, mice injected with S1P/JS-K/Lipo (**Figure 5**a). At 24 h postinjection with these different liposome formulations, brains with tumor tissues were resected. Histological analysis and blood vessel examination of the resected tissues revealed that S1P/JS-K/DiO-Lipo (green) were significantly colocalized with blood vessels (red) in the glioma tumor region at 24 h postinjection, whereas the intensity of the DiO-Lipo and JS-K/DiO-Lipo groups were weak (Figure 5b). As time extended to 96 h, S1P/JS-K/DiO-Lipo not only was clearly present in the vasculature but also had diffused away from the vessels, with clear dispersal in the brain glioma

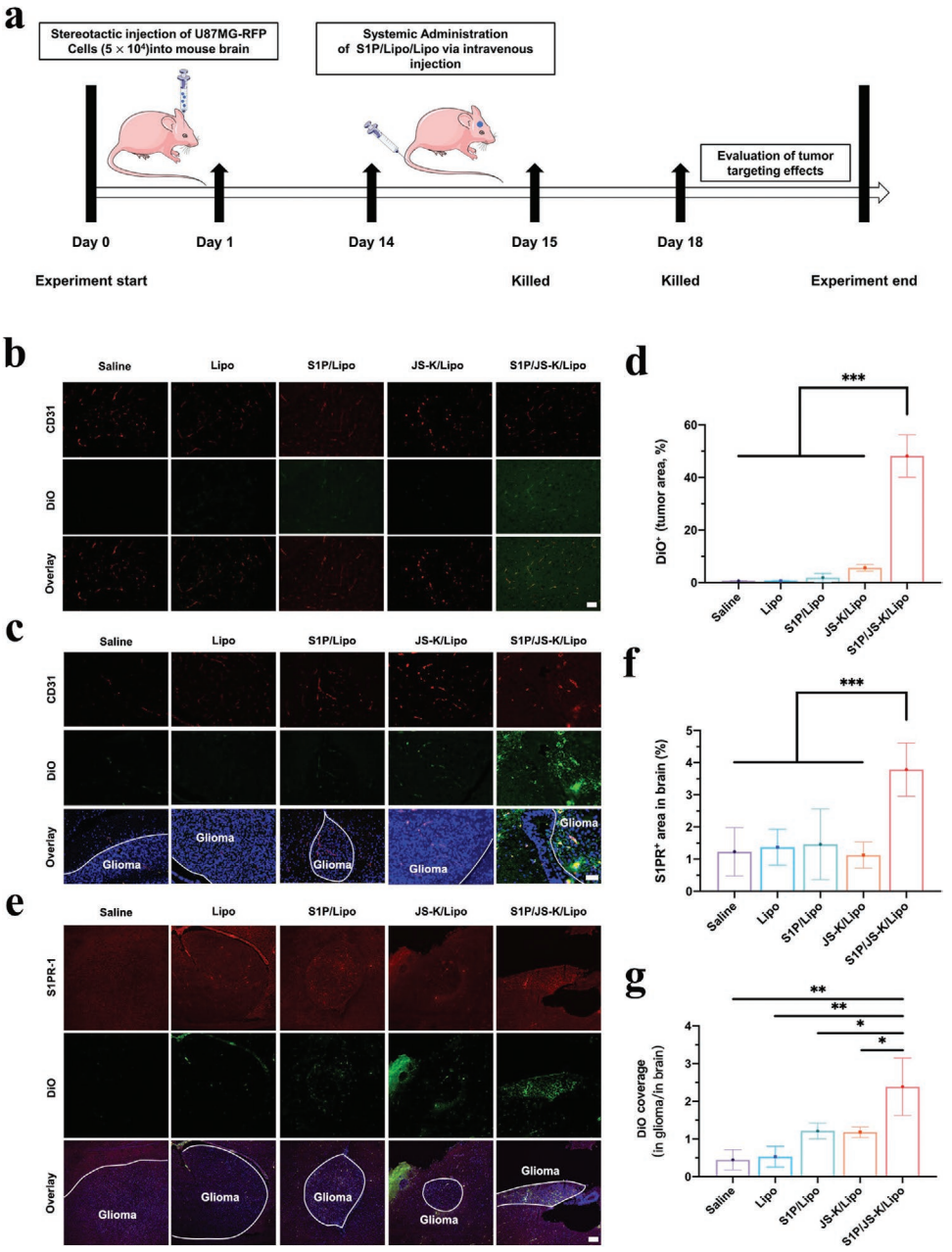

Figure 5. S1P/JS-K/Lipo enhanced the tumor-infiltrating effect of liposomes in orthotopic glioma models. a) Treatment protocol of the experimental brain-glioma-tumor-bearing model. Fourteen days after intravenous injection of U87MG-RFP (5.0×10^4 cells in 20 µL PBS), mice were treated with saline, Lipo, S1P/Lipo, JS-K/Lipo, or S1P/JS-K/Lipo. Experimental penetration and glioma tumor targeting effects of S1P/JS-K/Lipo were analyzed and quantified by monitoring the fluorescence locations of S1P/JS-K/Lipo with bEnd.3 cells at day 15 (24 h postinjection) and day 18 (96 h postinjection): saline, $n = 8$ mice; Lipo, $n = 8$ mice; S1P/Lipo, $n = 8$ mice; JS-K/Lipo, $n = 8$ mice; S1P/JS-K/Lipo group, $n = 8$ mice. b) Brains of mice were dissected and sectioned 24 h after treatment. Brain slices were stained with anti-CD31 antibody (red) for bEnd.3 cells and biodistribution of liposome formulations (green) in brain glioma regions were observed by CLSM. Scale bar: 20 µm. c,d) Brains of mice were dissected and sectioned 96 h after treatment. Brain slices were stained with anti-CD31 antibody (red) for bEnd.3 cells, and the biodistribution of liposomes (green) in brain glioma region was observed by CLSM, with quantification using ImageJ. Error bars: mean ± SD ($n = 5$). $^{***}P < 0.001$, in comparison with the S1P/JS-K/Lipo group using a one-way analysis of variance (ANOVA). e–g) Glioma tumor penetration analysis: mice bearing glioma tumors were treated with saline, DiO-Lipo, S1P/DiO-Lipo, JS-K/DiO-Lipo, or S1P-FITC/JS-K/Lipo. The tumors were dissected and sectioned at 96 h after treatment. The liposome formulations are shown in green, the cellular nuclei are stained with DAPI and shown in blue, and the S1PR immunofluorescence was shown in red. Error bars: mean ± SD ($n = 5$). $^{*}P < 0.05$, $^{**}P < 0.01$, and $^{***}P < 0.001$, in comparison with the S1P/JS-K/Lipo group in (f) and (g) using a one-way analysis of variance (ANOVA). Scale bars: 100 µm.

region (Figure 5c,d). These results indicate that the presence of the S1P targeting lipid greatly facilitates enhanced brain glioma tumor penetration of S1P/JS-K/Lipo, which our data shows is capable of penetrating the BBTB in vivo.

To assess the distribution ratio of S1P/JS-K/Lipo within glioma tumors after the BBTB penetration, S1PRs on glioma cells were stained with a S1PR antibody (Figure 5e). After 96 h, S1P/JS-K/DiO-Lipo signals colocalized with the S1P receptor-1 expressing glioma tumor regions in vivo: the entire glioma tumor region exhibited a nearly equivalent fluorescence intensity. In contrast, the JS-K/DiO-Lipo formulation was still restricted to the blood vessels (Figure 5f,g), highlighting the superior glioma tumor-penetrating ability of S1P/JS-K/Lipo.

2.9. S1P/JS-K/Lipo Showed Enhanced Accumulation in Glioma Areas In Vivo

We also performed detailed imaging analysis in U87MG-RFP-tumor-bearing nude mice to further characterize the enhanced accumulation of red fluorescence labeled S1P/JS-K/DiR-Lipo in the glioma area (**Figure 6**a). After intravenous injection for 4 h, the S1P/JS-K/DiR-Lipo exhibited a clear fluorescence signal in the brain glioma region (Figure 6b). As time extended to 48 h, S1P/JS-K/DiR-Lipo presented significantly stronger fluorescence at the in situ brain tumor postadministration, compared to brains of JS-K/DiR-Lipo- or S1P/DiR-Lipo-treated mice. The fluorescence intensity in the brain of the S1P/JS-K/DiR-Lipo-treated mice was 1.8- and 2-fold higher than the JS-K/DiR-Lipo and DiR-Lipo groups, respectively (Figure 6c). Thus, S1P/JS-K/DiR-Lipo demonstrates a superior glioma tumor-targeting ability compared to JS-K/DiR-Lipo and DiR-Lipo.

Brains tissues were collected at 48 h and ex vivo imaging was used to assess potential colocalization of the S1P/JS-K/DiR-Lipo fluorescence signal with the luminescence expressed by the U87MG-RFP cells themselves. DiR-Lipo did not accumulate in large amounts in the brain due to obstruction by the BBTB, with the accumulation effect slightly improved after encapsulation via free JS-K. Although S1P/Lipo exhibited a targeting effect on glioma cells, the intensity of its accumulation in the glioma region was low, whereas S1P/JS-K/Lipo very clearly accumulated in large quantities within the brain glioma region, and the fluorescence signal of S1P/JS-K/Lipo exhibited colocalization with the luminescence signal of U87MG-RFP cells (Figure 6d).

As shown in Figure 6e, we then used the G/B ratio as an index to evaluate the selective accumulation capacity of S1P/JS-K/DiR-Lipo, namely, the fluorescence signal of the dye-labeled liposome formulation in the glioma site relative to that in the brain parenchyma. The glioma to brain (G/B) ratio of DiR/S1P/JS-K/Lipo was 4.75, which was substantially higher than saline (1.96), DiR-Lipo (1.71), S1P/DiR-Lipo (2.96), or JS-K/DiR-Lipo (2.11). S1P/JS-K/DiR-Lipo's higher fluorescence signal confirmed its superior in vivo brain-tumor targeting ability over DiR-Lipo, S1P/DiR-Lipo, and JS-K/DiR-Lipo, implicating the importance of S1P receptor-mediated effects.

2.10. Increased Blood Flow in the GBM Tumor Microenvironment upon Treatment with S1P/JS-K/Lipo

Along with the improved targeting ability of liposomes in the brain region, as shown in the color-code images and quantitative analysis of blood flow in Figure 6f,g, it was clear that unlike the control groups injected with Lipo or saline, the JS-K/Lipo-treated tumors had undergone recanalization after 6 h, which was maintained up to 24 h. However, the increased blood flow in the brain was present after only 2 h postinjection in the S1P/JS-K/Lipo group. These results show that the GST-mediated catalysis of NO molecules from the JS-K prodrug substrate promoted vasodilation, creating a cumulative treatment effect by further increasing the size of gaps between the BBTB endothelial cells.

2.11. S1P/JS-K/Lipo Enabled Enhanced Ultrasound Imaging in Glioma Areas In Vivo

NO gas bubbles production from S1P/JS-K/Lipo accumulated in the tumor area was further assessed via ultrasound imaging. Following S1P/JS-K/Lipo injection, the mice tumor area showed strong acoustic signals, owing to NO generation, with distribution throughout the whole glioma tumor region after 12 h (Figure S9, Supporting Information), displaying strong signals for irregular circular areas. The signals observed in tumors from mice treated with JS-K/Lipo were substantially weaker and could only be observed in the marginal region of the glioma due to weak penetration into the tumor area; the treatment exhibited a ring-shaped area of acoustic signal (Figure 6h). Based on the quantitative analysis of ultrasonic intensity (Figure 6i), we determined a consistent trend when the ultrasonic images began to strengthen with the accumulation of the liposomes in the brain region in the in vivo fluorescence imaging experiment.

2.12. Accumulated S1P/JS-K/Lipo Exhibited Enhanced Therapeutic Effects against Glioma Tumors

We further evaluated the antitumor activities of S1P/JS-K/Lipo using U87MG-RFP-tumor-bearing mice. When tumor masses were around 50 mm^3 (generally 14 days after tumor cell implantation), we intravenously injected the mice with: S1P/JS-K/Lipo (equivalent to 2×10^{-3} mg kg^{-1} body weight of S1P and 1 mg kg^{-1} body weight of JS-K), S1P/Lipo, JS-K/Lipo, Lipo, or saline. The injections were given at an interval of 10 days, for a total of 5 treatments (**Figure 7**a).

The S1P/JS-K/Lipo presented a clearly superior accumulative effect in glioma brain areas compared to the Lipo, S1P/Lipo, and JS-K/Lipo groups (Figure S10, Supporting Information). The S1P/JS-K/Lipo levels in brain regions achieved a 2.4-fold improvement once the treatment was terminated. The continuous accumulation of S1P/JS-K/Lipo in the glioma region promoted the subsequent release of NO, clearly distributed inside the glioma tumor region to enhance blood flow (Figure S11, Supporting Information). Ultrasound imaging demonstrated that liposomes had completely infiltrated the entire brain glioma region after intravenous S1P/JS-K/Lipo injection (Figure S12, Supporting Information).

Tumor growth was significantly inhibited after S1P/JS-K/Lipo treatment, and the fluorescence intensity and distribution area of glioma tumor cells exhibited a decreasing trend (Figure 7b,c) compared to the control groups injected with saline or Lipo.

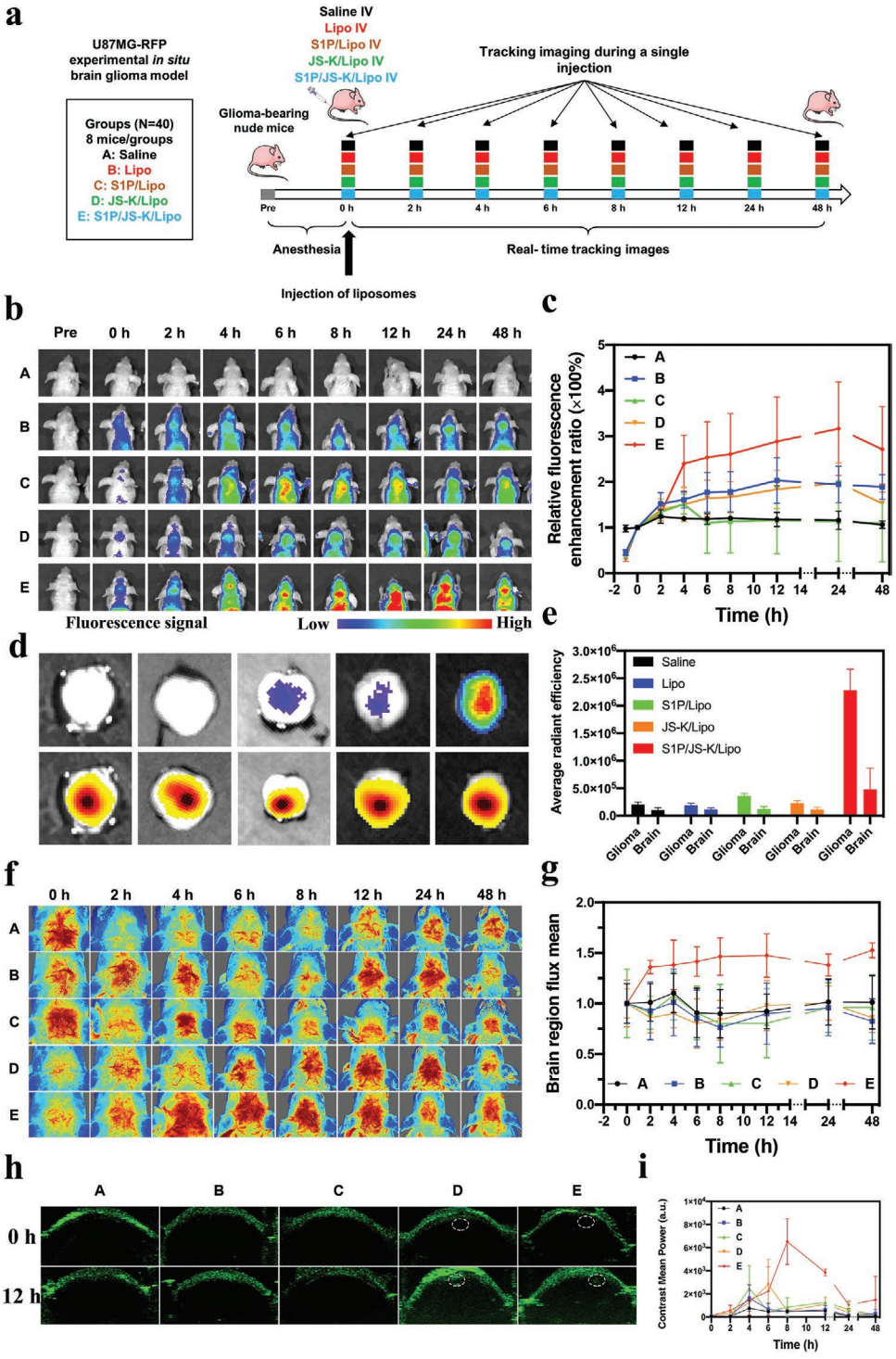

Figure 6. In vivo distribution of S1P/JS-K/Lipo. a) Schematic illustration of the treatment protocol and timeline for the in vivo distribution and delivery experiments. Two weeks after the implantation of U87MG-RFP cells (1×10^6 cells in situ injection), mice were given intravenous injections of differing liposome formulations (A, saline; B, Lipo; C, S1P/Lipo; D, JS-K/Lipo; E, S1P/JS-K/Lipo, $n = 8$ mice for each group). b) In vivo fluorescence images of the: A) vehicle-treated mice, B) Lipo mice, C) S1P/Lipo mice, D) JS-K/Lipo mice, and E) S1P/JS-K/Lipo mice. c) ROI analysis of the averaged fluorescence intensity from the brain tumors of the: A) vehicle control mice, B) Lipo mice, C) S1P/Lipo mice, D) JS-K/Lipo mice, and E) S1P/JS-K/Lipo mice. Error bars: mean ± SD ($n = 8$ mice per group). The area under the curve density versus time in the brain for the DiR signal of S1P/JS-K/Lipo group mice was significantly higher than that of the other four groups. d) Ex vivo fluorescence images of brains collected 48 h after intravenous injection of liposome formulations: top row represents the fluorescence signals of accumulated liposome formulations; lower row represents in situ bioluminescence of glioma tumors. e) The semiquantitative data for the fluorescence signal, at sites indicated in (d). Error bars: mean ± SD ($n = 8$ mice per group). f) Changes in blood flow in the brain regions of the U87MG-RFP-tumor-bearing mice, after treatment with the indicated liposome formulations. g) Quantitative

S1P/JS-K/Lipo treatment led to tumor regression in almost all the mice after 5 treatments. No noticeable reduction in mice body weight occurred during S1P/JS-K/Lipo treatment, whereas mice weights exhibited a steady decreasing trend when treated with the other liposome formulation (Figure 7d). The saline and Lipo-treated U87MG-RFP-bearing mice groups had 50% mortality rates at day 12 and day 13, respectively (Figure 7e), with no significant change in survival rate upon treatment with S1P/Lipo or JS-K/Lipo. The longest survival for the U87MG-bearing mice occurred in the S1P/JS-K/Lipo group: 50% survival at 22 days. Therefore, S1P/JS-K/Lipo exerts superior antitumor activity to JS-K/Lipo or free JS-K.

2.13. Therapeutic Evaluation by Histopathological Analysis

Finally, we conducted histological analysis to examine any changes in the vascular distribution and/or tumor morphology of glioma after the treatment. There was no damage to major organs (heart, liver, spleen, lung, or kidney) observed for the saline, Lipo, S1P/Lipo, JS-K/Lipo, or S1P/JS-K/Lipo groups, supporting the apparent safety of these liposome formulations (Figure S13, Supporting Information).

Microscopy of brain sections from the different treatment groups showed that the vessels in the glioma region of mice injected with S1P/Lipo and JS-K/Lipo grew slowly, whereas the vessel density in the glioma region of mice injected with S1P/JS-K/Lipo decreased significantly after multiple injections, indicating that tumor development was inhibited. The vascular density in the glioma region of the brains of nude mice injected with saline or Lipo increased significantly over time; additionally, their vascular morphology changed with enlarged lumens and thickened walls, tumor cells clustered significantly around small- and medium-sized vessels (Figure 7f). Consistent with the results of vascular immunohistochemical staining, the glioma collected from the S1P/JS-K/Lipo-treated mice exhibited a round shape and a well-delimited margin, and these animals showed no signs of local infiltration into the normal brain parenchyma (Figure 7g). In contrast, tumors collected from mice treated with the other formulations all had irregular shapes, and the brains of these animals all had margins with obvious tumor cells infiltration.

3. Conclusion

Glioblastoma is a highly aggressive central nervous system cancer. Accumulating evidence supports that high levels of S1P and aberrantly elevated S1P receptors expression can induce S1P-signaling in GBM and may promote the sustained proliferation, invasive behavior, cell death resistance, immune evasion, and dysregulated energy metabolism of tumor cells, as well as increased tumor angiogenesis.[43–45] Accordingly, targeting S1P has emerged as an attractive potential strategy for therapies against GBM. Herein, we successfully developed a phospholipid-signaling sphingolipid hybrid and GST-responsive liposomal dosage that is able to deliver the therapeutic prodrug JS-K specifically and safely into GBM tumors. We observed that during JS-K/S1P/Lipo's entrance into tumor endothelial cells and triggering specific S1P interactions with S1PRs on endothelial cells, it enabled Caveolae-1-mediated enhanced transendothelial transcytosis via *P*-gp inhibition. After overcoming the BBTB, JS-K/S1P/Lipo specifically interacted with gliomas cells mediated by high S1P receptor levels.

Following the targeted delivery and release of NO donor JS-K molecules to the GBM microenvironment, NO gas is produced via enzymatic activation by overexpressing GST in glioblastoma. NO has been identified previously as a promising therapeutic strategy.[46–48] We utilized nondestructive ultrasound imaging and observed GST-mediated catalysis of JS-K into cytotoxic microsized NO bubbles in the vasculature of GBM tumors. Large quantities of microsized NO bubbles were continuously generated via a GST enzymatic trigger and, for the first time, we quantified this NO production by ultrasound imaging visualization.

Looking beyond this initial use of our S1P-liposomes for delivering JS-K, there is no obvious limitation preventing the further development of this liposomal system for a variety of other therapeutic applications; for example, the delivery of anti-inflammatory agents to glioma vessels or delivery of small-molecule anticancer drugs to other carcinomas that feature elevated S1PR expression. This paper provides the foundation for an exciting new avenue of cancer therapeutics.

4. Experimental Section

Materials and Methods: O_2-(2,4-dinitrophenyl) 1-[(4-ethoxycarbonyl) piperazin-1-yl] diazen-1-ium-1,2-diolate (JS-K, molecular weight (M_w = 384.30)), S1P, FITC covalently modified S1P (S1P-FITC), 1,2-dipalmitoyl-sn-glycero-3-phosphocholine (DPPC), 1,2-distearoyl-sn-glycero-3-phosphocholine (DSPC), 1,2-distearoyl-sn-glycero-3-phosphoethanolamine-*N*-[methoxy(poly(ethylene glycol))-2000] (DSPE-mPEG2000), L-glutathione reduced (GSH), and glutathione *S*-transferase were all purchased from Sigma-Aldrich (USA). DAF-FM DA, 3,3′-dioctadecyloxacarbocyanine perchlorate (DiO), 1,1′-dioctadecyl-3,3,3′,3′-tetramethylindotricarbocyanine Iodide (DiR), and 1,1′-dioctadecyl-3,3,3′,3′-tetramethylindocarbocyanine perchlorate (DiI) were purchased from Beyotime (Haimen, China). Antibodies and fluorescently labeled secondary antibodies used: caveolin-1 monoclonal antibody (Beyotime, Haimen, China), Alexa Fluor 647-labeled Goat IgG (H+L) (Abcam; catalogue no: ab150115), antimouse CD31 (Abcam; catalogue no: ab28364), Alexa Fluor 555-labeled Goat IgG(H+L) (Abcam; catalogue no: ab150078), and antimouse S1PR1 (Abcam; catalogue no: ab11424). Dulbecco's modified Eagle's medium (DMEM), fatal bovine serum (FBS), and CCK-8 were obtained from Gibco (Thermo Fisher Scientific, USA). Other reagents and materials were purchased from Sigma-Aldrich unless otherwise noted.

Preparation of Liposomal Formulations: S1P/JS-K/Lipo were produced via the thin-film hydration and membrane-filtering extrusion method. Briefly, for blank Lipo (without drug or dye loading), a mixture of DPPC/DSPC/DSPE-mPEG2000 (90/5/5 in molar ratio) in $CHCl_3$ was

analysis of blood flow in the brain shown in (f). Error bars: mean ± SD (n = 8 mice per group). h) Time-dependent in vivo representative brain glioma tumor ultrasound images after i.v. injection of various liposome formulations. i) The average gray value of contrast-enhanced ultrasound imaging over time: following injection of saline, Lipo, S1P/Lipo, JS-K/Lipo, or S1P/JS-K/Lipo. Error bars: mean ± SD (n = 8 mice per group).

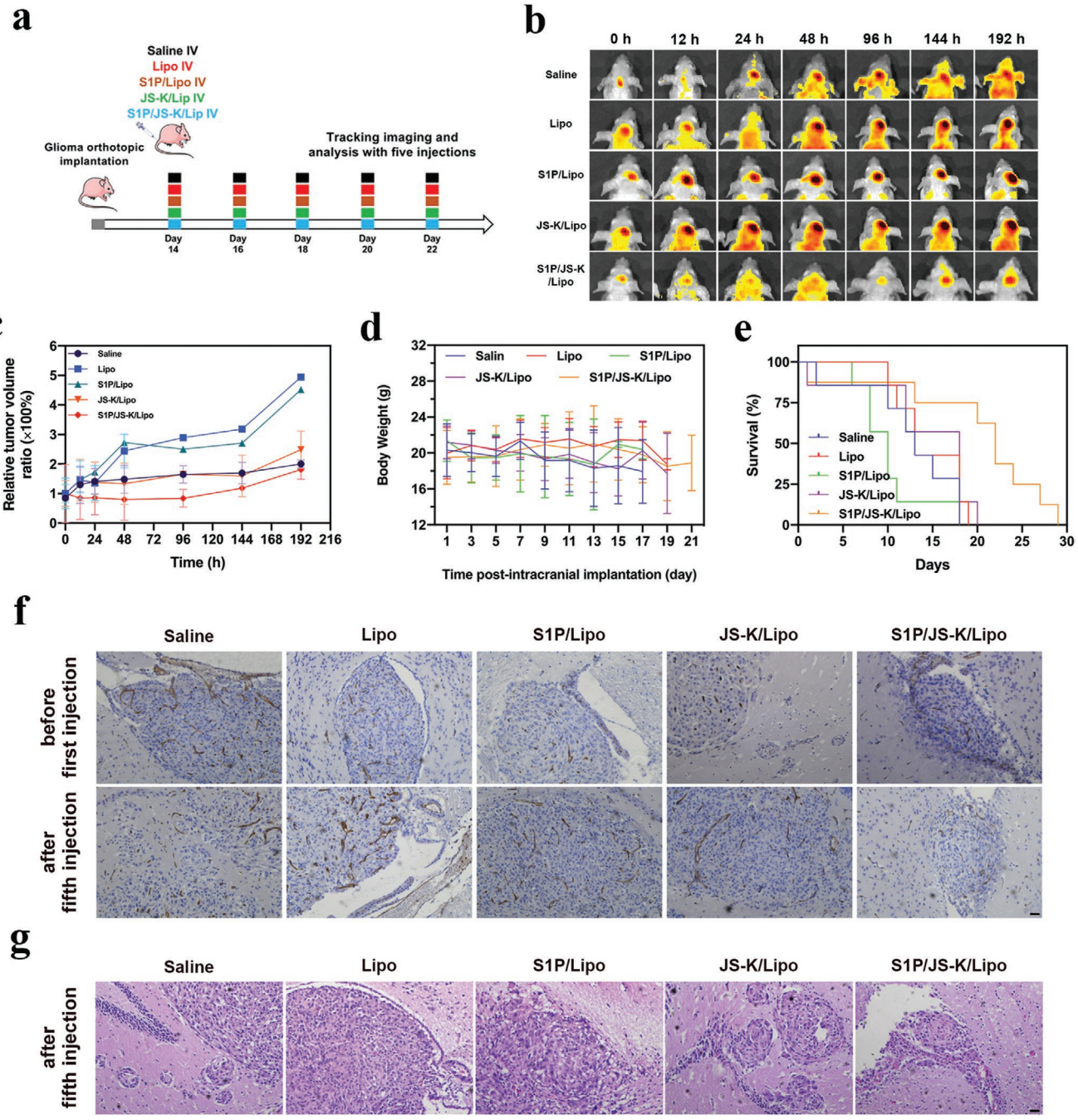

Figure 7. Antitumor efficacy of S1P/JS-K/Lipo. a) Experimental timeline for the administration of liposomes in a mouse model of glioblastoma (U87MG-RFP cells) by tail vein injection. b) Time course of RFP fluorescence images of the U87MG-RFP-bearing mice after receiving indicated injections with saline, Lipo, S1P/Lipo, JS-K/Lipo, or S1P/JS-K/Lipo. Data are shown as mean ± SD (n = 8 independent experiments). c) Quantitative chart showing the total fluorescence intensities of the brain tumor regions of the indicated mice groups. Error bars: mean ± SD (n = 8 mice per group). d) Change in body weights of the U87MG-RFP-bearing mice after treatment with different liposome formulations. Error bars: mean ± SD (n = 8 mice per group). e) Median survival curve of the U87MG-RFP-tumor-bearing mice after treatment with saline, Lipo, S1P/Lipo, JS-K/Lipo, or S1P/JS-K/Lipo (n = 8 mice per group). f) CD31 immunohistochemical staining of U87MG-RFP glioma tumors dissected from mice given 5 treatments with the indicated liposome formulations. Scale bar: 20 µm. g) H&E staining of brains from U87MG-RFP-bearing mice. Scale bar: 20 µm.

rotary evaporated to form a thin film. Any residual organic solvent was removed by overnight evaporation under vacuum. The dried lipid film was subsequently hydrated with saline at 60 °C for 30 min, and the lipid dispersion was extruded through polycarbonate membranes with the pore size ranging from 400 to 100 nm.

JS-K loaded liposomes (including JS-K/Lipo, S1P/JS-K/Lipo, and S1P-FITC/JS-K/Lipo) were prepared using a traditional passive loading method. Briefly, a mixture of DPPC/DSPC/DSPE-mPEG2000/JS-K, DPPC/DSPC/DSPE-mPEG2000/JS-K/S1P, or DPPC/DSPC/DSPE-mPEG2000/JS-K/S1P-FITC in $CHCl_3$ was rotary evaporated to form a

thin film. The subsequent protocol was similar to blank liposomes. After extrusion, free JS-K, S1P, or S1P-FITC were removed by G50 column.

Evaluation of Physical Properties of S1P/JS-K/Lipo: The morphology, size, polydispersity, and temporal stability of S1P/JS-K/Lipo were evaluated. The hydrodynamic sizes and polydispersity indices (PDIs) of different formulations (Lipo, JS-K/Lipo, S1P/JS-K/Lipo, and S1P-FITC/JS-K/Lipo) were measured using a Zeta-Sizer Nano-ZS 90 (Malvern Instruments, UK). The zeta potential of the formulations was determined after a fivefold dilution by laser Doppler velocimetry using a Nanosizer ZS with a universal dip cell (Malvern Instruments, UK). Each sample was measured in triplicate.

Surface morphology was determined by TEM (JEM-2100, JEOL, Japan). In brief, liposome samples (10 µL) were dropped onto copper 200-mesh grids. After draining via a filter paper for 30 min, a phosphotungstic acid stain solution (1.5% by weight, adjusted to pH 6.0) was applied for 10 min and TEM images were taken.

To demonstrate that JS-K had been loaded into the liposomes, freshly prepared liposomes (Lipo, JS-K/Lipo, and S1P/JS-K/Lipo) were lyophilized via freeze dryer (AdVantage2.0, SP Scientific, USA). The dry powders were scanned in the 400 to 4000 cm^{-1} wavelength range using an FT-IR spectrophotometer (IRAffinity-1, Shimadzu Corporation, Japan).

The content of JS-K in JS-K/Lipo, S1P/JS-K/Lipo, and S1P-FITC/JS-K/Lipo was determined using HPLC. Briefly, freshly prepared liposomes were mixed with 9 equivalent of methanol solution (by volume) and then vortexed for 5 min to fully destroy the liposome structure and release JS-K from the liposomes. After filtration via a 200 nm membrane, the solution (20 µL) was measured by an HPLC system with a Phenomenex Luna 5 C18 column (Torrance, CA). The mobile phase was water (containing 0.1% formic acid) at a flow rate of 1 mL min^{-1} (percentage of acetonitrile: 25% for 0–5 min followed by a linear program to 70% at 15 min). The concentration of the drug encapsulated inside the liposomes was calculated based on a JS-K standard concentration curve.

Release of JS-K from S1P/JS-K/Lipo: The in vitro release properties of JS-K from S1P/JS-K/Lipo were evaluated in PBS with GSH and different concentration of GST; GST was added into PBS to simulate its stimulated release in blood circulation and at tumor sites, respectively. Briefly, 5 mL of the purified S1P/JS-K/Lipo solution was sealed into a dialysis bag (MWCO, 3.5 kDa) and placed in 30 mL PBS (pH 7.4) containing GSH (200 mg L^{-1}) and differing concentrations of GST (0.53 ng mL^{-1} for simulated blood and 3.57 ng mL^{-1} for simulated cancer cells) with gentle mixing (200 rpm) at 37 °C. At predetermined time intervals (0, 1, 2, 3, 4, 5, 6, 7, and 8 h), 100 µL S1P/JS-K/Lipo solution was withdrawn from the dialysis bag and replaced with 100 µL of fresh buffer solution. Then, the JS-K not released from S1P/JS-K/Lipo was measured by HPLC and calculated via standard curves. Subsequently, the released percentage of JS-K was calculated according to Equation (1)

$$\text{Release percentage} = \frac{C_{\text{loading}} - C_{\text{remaining}}}{C_{\text{loading}}} \times 100\% \quad (1)$$

where C_{loading} is the total JS-K loading concentration of intact S1P/JS-K/Lipo, and $C_{\text{remaining}}$ is the remaining JS-K concentration of S1P/JS-K/Lipo in dialysis bag during release process at each time point.

Cell Culture: Glioma cells (cell line U87MG) were obtained from the Shanghai Institute of Cell Biology (Shanghai, China). The mouse brain capillary endothelial cell line bEnd.3 was purchased from Jennio Biotech Co., Ltd. (Guangzhou, China). All these cells were cultured in DMEM (Gibco, USA) supplemented with 10% FBS (Gibco, USA) and 100 µg mL^{-1} penicillin/streptomycin in a humidified atmosphere of 5% CO_2 at 37 °C. Culture medium was refreshed every 2–3 days. When the cells reached 70–80% confluence, they were digested with 0.25% trypsin–EDTA solution, harvested by centrifugation, and resuspended in PBS for experimental use.

In Vitro Cell Cytotoxicity Assay: The cytotoxicity of free JS-K, Lipo, JS-K/Lipo, and S1P/JS-K/Lipo for bEnd.3 cells and U87MG cells were determined via CCK-8 cell proliferation assay based on a modified manufacturer's protocol. Briefly, bEnd.3 cells or U87MG cells were seeded with 96-well plates at a density of 5×10^3 cells per well and were cultured overnight, followed by the addition of the free JS-K, JS-K/Lipo, and S1P/JS-K/Lipo at several concentrations (equivalent to 1, 2.5, 5.0, 10.0, 15.0, and 20.0 µg mL^{-1} of JS-K). After an additional 24 h incubation, CCK-8 solution (10 µL) in medium (90 µL) was added to each well and incubated for another 1 h. The absorbance intensity in each well was measured at 450/650 nm by using a multimode microplate reader Infinite M200 PRO (Tecan instruments, USA).

In Vitro NO generation and Characterization: In order to detect the generation process of NO in cells incubated with liposome formulations, the NO fluorescent probe DAF-FM DA was pretreated with the cells at a final concentration of 5×10^{-6} M. After incubation in a 37 °C incubator in the dark, the unloaded fluorescent probe was removed by three times PBS washes. Then, differing liposome formulations (200 µL) were added to the Petri dish, and an optical microscope (TS100/TS100-F, Nikon Co., Ltd., Japan) was used to monitor real-time NO generation at set time intervals (pre, 0.5, 1, 2, and 4 h).

Flow Cytometry Measurement: Cells (1.5×10^4 per well) were seeded into 12-well plates and incubated for 24 h; DiO-Lipo, S1P/DiO-Lipo, JS-K/DiO-Lipo, or S1P-FITC/JS-K/Lipo solution was added to each well and incubated for timed intervals. The cells were then trypsinized, washed three times with cold PBS, and resuspended in 0.5 mL PBS. The cells were immediately analyzed by flow cytometry (NovoCyte D2040R, ACEA Biosciences, Singapore). Files were collected for 10 000 gated events and three independent duplicate experiments were conducted.

Transcellular Delivery of S1P/JS-K/Lipo: The in vitro BBTB model was constructed with bEnd.3 cells using the Transwell cell culture system (Corning, USA). bEnd.3 cells (1×10^5 cells per well) were seeded onto the upper chamber of the Transwell and cultured with medium containing FBS (10% v:v); U87MG cells were seeded onto the lower chamber. The integrity of the cell monolayer was evaluated by measuring transendothelial electrical resistance (TEER) values using a Millicell-ERS voltammeter (Millipore, USA). The cell monolayers with TEER values higher than 300 Ω cm^2 were used as the BBTB model for the transmigration studies.

The Transwell system was then incubated in a cell incubator for 48 h. After, bEnd.3 cells grown in the upper chamber were incubated with DMEM medium with the addition of S1P-FITC/JS-K/Lipo, JS-K/DiO-Lipo, or DiO/Lipo, respectively. At predetermined intervals (0, 2, 4, 6, 8, 10, 12, and 24 h), the U87MG cells in the lower chamber were collected, the medium replaced with fresh medium, and the cell membranes stained with DiI (10×10^{-6} M) dye for 10 min. The transendothelial process of S1P-FITC/JS-K/Lipo, JS-K/DiO-Lipo, and DiO-Lipo were observed using a Leica SP8 confocal laser scanning microscopy system.

Effects of Caveolin-1 and P-gp on Cellular Uptake of S1P/JS-K/Lipo: bEnd.3 cells were seeded into 12-well plates to reach 60–80% confluency after overnight incubation. The medium was replaced with fresh medium and subsequently three type of liposomes (DiO-Lipo, JS-K/DiO-Lipo, and S1P-FITC/JS-K/Lipo) were respectively added into the medium. After incubation to various timepoints (0, 2, 4, 6, 8, 10, 12, and 24 h), the media was removed and the cells washed with PBS three times. The cells were then blocked with immunologic staining blocking buffer for 1 h at room temperature and incubated with primary antibodies against caveolin-1 or *P*-glycoprotein at 4 °C overnight. Cells were washed with PBS and incubated with Alexa Fluor 647 or 555 antirabbit IgG secondary antibodies for 1 h at room temperature. Afterward, all cells were washed with PBS before imaging by a confocal laser scanning microscope (FV3000, Olympus).

In Situ Glioma Tumor Model: BALB/c nude male mice were purchased from Shanghai SLAC Laboratory Animal Co., Ltd. (Shanghai, China). All mice were 6–8 weeks old and kept under specific pathogen free (SPF) conditions in a 12 h light–dark cycle, a room temperature of 20–22 °C, and a humidity of 40–60% for at least 1 week to adapt the experimental conditions. All animal experiments, animal care, and animal model protocols were approved by the Committee on the Ethics of Animal Experiments of the Institute of Process Engineering at the Southeast University (NO. 20200409006).

The human glioma cells U87MG-RFP, expressing red fluorescent protein (RFP), were used to establish the in situ glioma tumor model.

Mouse xenografts were generated in 8-week-old BALB/c mice by stereotactic intracranial implantation of 1×10^6 cells into the brain parenchyma of nude mouse through a craniotomy open window. At 14 days postimplantation, mice with similar bioluminescence intensities of glioma in brain regions, as measured by IVIS Spectrum In Vivo Imaging System (PerkinElmer, USA), were randomized in five groups ($n = 8$ per group) for collection and analysis: Group 1, mouse model injected with saline; Group 2, mice injected with Lipo; Group 3, mice injected with S1P/Lipo; Group 4, mice injected with JS-K/Lipo; and Group 5, mice injected with S1P/JS-K/Lipo.

Small-Animal Ultrasound Imaging of Brain Tumor: S1P/JS-K/Lipo, JS-K/Lipo, S1P/Lipo, Lipo, and saline groups were prepared and intravenously injected into nude mice bearing U87MG-RFP tumors. Before acoustic imaging, mice were anesthetized by intraperitoneal administration of a 150 mg kg^{-1} sodium pentobarbital solution (10 µL g^{-1} body weight). Then, the tumor was imaged with a high-resolution microimaging system (VisualSonics Vevo 2100, Canada) with the transducer at 18 MHz using both B-mode and contrast mode. B-mode imaging settings: center frequency 18 MHz, intensity power 100%, and contrast gain 18 dB. Contrast mode imaging settings: center frequency 18 MHz, intensity power 4%, and contrast gain 35 dB. A gray-scale mapping function was used to calibrate the ultrasound video intensity to ensure the video-image results were in the linear region. The mean video intensity in the regions of interest (ROIs) of the tumor were analyzed and normalized to the video intensity at the time of contrast agent injection (time = 0). Time-dependent ultrasound imaging was monitored at different time points (0, 2, 4, 6, 8, 12, and 24 h) after sample injection.

Blood Flow Reperfusion Measurement in the Brain Tumor Area: Nude mice bearing U87MG-RFP tumors ($n = 8$) were anesthetized by intraperitoneal administration of a 150 mg kg^{-1} sodium pentobarbital solution (10 µL g^{-1} body weight). The cerebral blood flow (CBF) in the whole brain area of tumor-bearing mice injected with S1P/JS-K/Lipo, JS-K/Lipo, S1P/Lipo, Lipo, and saline were assessed using a full-field laser perfusion imager (FLPI-2 Pro, Moor Instruments, UK). The CBF images were captured, and changes in blood flow in the brain area after intravenous injection were recorded at predetermined time intervals (0, 2, 4, 6, 8, 12, and 24 h) using MoorFLPI software.

Biodistribution of Liposomes In Vivo and Therapeutic Evaluation with Histology and Immunohistochemistry Analysis: To characterize the beneficial therapeutic effects and enhanced penetration capability of S1P/JS-K/Lipo on BBTB, mice were weighed at regular intervals after treatment with fluorescently labeled S1P/JS-K/DiR-Lipo, JS-K/DiR-Lipo, S1P/DiR-Lipo, DiR-Lipo, or saline, respectively, via tail-vein injection. At predetermined time interval postadministration, the mice were imaged using an in vivo optical imaging system (IVIS Spectrum Imaging System, Caliper Life Sciences, USA). To study tissue biodistribution, mice were sacrificed postinjection and the major organs excised and captured by a near-infrared fluorescence in vivo imaging system.

The harvested tumor and main organ tissues were fixed in 4% neutral buffered paraformaldehyde and embedded in paraffin. The paraffin-embedded tumors and organs were further cut into slices at a thickness of 10 µm for hematoxylin and eosin (H&E) staining. For H&E staining observation, the major organs (brain, liver, spleen, lung, and kidney) in each group were dehydrated and subsequently embedded with paraffin. Tissue sections of 5 µm thickness were prepared after being embedded in paraffin, sectioned, and deparaffinization. Then, organ sections were obtained and stained by H&E. The results were examined by a bright-field TS100/TS100-F optical microscope (Nikon, Japan).

For the immunohistochemical studies, brains with tumor tissues (U87MG-RFP) were harvested, fixed in 4% neutral buffered paraformaldehyde, embedded in paraffin, and then prepared into serial sections (6 µm). Subsequently, the sections were dewaxed and rehydrated with xylene, ethanol, and deionized water. Endogenous peroxidase was quenched with 3% hydrogen peroxide for 0.5 h and then rinsed with deionized water, followed by blocking with 10% normal goat serum for 1 h. Next, the slides were stained with rabbit antihuman CD31 overnight at 4 °C, and then reacted with horseradish peroxidase-conjugated secondary antibody for 1 h at room temperature. Diaminobenzidine was used as the substrate to produce an observable brown color.

Intertumoral Distribution of S1P/JS-K/Lipo: DiO-labeled liposomes, S1P/Lipo, JS-K/Lipo, and S1P-FITC/JS-K/Lipo were injected into glioma-tumor-bearing nude mice via the tail vein. After 24 h, brains were harvested, dehydrated, and embedded in paraffin. Then, brain tissues were cut into 5 µm thick sections, and microvessels were labeled with anti-CD31 antibodies (Abcam, ab28364) or anti-S1PR1 antibodies (Abcam, ab111571) overnight at 4 °C. After blockage with 3% BSA for 1 h, Alexa Fluor 555-conjugated secondary antibodies (Abcam, ab150078) were used to stain for 1 h at 37 °C. The brain tissues were then stained with 4′,6-diamidino-2-phenylinodle (DAPI)-containing mounting medium for 10 min at room temperature. Sections were then observed by FV3000 confocal microscopy (Olympus, Japan). ImageJ software (NIH, USA) was used to quantify brain distribution of liposomes.

In Vivo Antitumor Activity: Once glioma luminescence could be observed via an IVIS Spectrum In Vivo Imaging System (PerkinElmer, USA), mice were randomly divided into five groups. The mice were treated intravenously (via the tail vein) with S1P/JS-K/Lipo, JS-K/Lipo, S1P/Lipo, Lipo, and saline, respectively. The treatment schedule was one injection every 2 days, to a total of five injections. Body weights were monitored at the time of each injection, as was tumor bioluminescence by the in vivo imaging system. Tumor size was measured every day with vernier calipers in three dimensions.

Mice were weighed at regular intervals after treatment. After euthanasia, tumors and major organs were excised and fixed in formalin for immunohistochemical analysis. Lesion sections were also stained with H&E or immunohistochemistry stains.

Suppression of Glioma Progression and Growth: The glioma-bearing mice were divided into five groups; the mice were treated intravenously with S1P/JS-K/Lipo, JS-K/Lipo, S1P/Lipo, Lipo, and saline, respectively, at 0, 2, 4, 6, 8, and 10 days. The body weights and survival periods of the mice were monitored during treatment. Histological analyses of brain sections were performed when symptoms of neurological compression of the mice was observed, such as aggravated hemiplegia and extreme malaise. The H&E-stained brain sections were visualized using an optical microscope.

Safety Evaluation: After treatment with different formulations, histological analyses on the major organs, including the heart, liver, spleen, lung, and kidney, using H&E staining were performed.

Statistical Analysis: Quantitative data were presented as means ± standard deviation (SD) from sample numbers (n). Data from experiments were analyzed using GraphPad Prism 8. Statistical comparisons were made by unpaired Student's t-test (between two groups) and one-way ANOVA (for multiple comparisons). P value <0.05 was considered statistically significant. For quantitative analysis in fluorescence intensity for confocal images, Image J software (National Institutes of Health, USA) was used for densitometric analysis.

Supporting Information

Supporting Information is available from the Wiley Online Library or from the author.

Acknowledgements

This investigation was financially funded by the project of the National Key Research and Development Program of China (2018YFA0704103 and 2017YFA0104302) and the National Natural Science Foundation of China (81971750 and 61821002), and partially by the National Natural Science Foundation of Jiangsu (BK20191266), the Six Talent Peaks Project of Jiangsu Province (2017-SWYY-006), and Zhong Ying Young Scholar of Southeast University. The authors would also like to thank the support from the Fundamental Research Funds for the Central Universities.

Conflict of Interest

The authors declare no conflict of interest.

Data Availability Statement

The data that support the findings of this study are available within the article and its supplementary material.

Keywords

caveolin, glioblastoma therapy, nitric oxide, *P*-glycoprotein, sphingosine-1-phosphate, ultrasound imaging

Received: March 2, 2021
Revised: April 10, 2021
Published online: June 9, 2021

[1] P. Wesseling, D. Capper, *Neuropathol. Appl. Neurobiol.* **2018**, *44*, 139.
[2] Q. T. Ostrom, G. Cioffi, H. Gittleman, N. Patil, K. Waite, C. Kruchko, J. S. Barnholtz-Sloan, *Neuro-Oncology* **2019**, *21*, v1.
[3] A. C. Tan, D. M. Ashley, G. Y. Lopez, M. Malinzak, H. S. Friedman, M. Khasraw, *Ca-Cancer J. Clin.* **2020**, *70*, 299.
[4] F. C. Lam, S. W. Morton, J. Wyckoff, T. L. V. Han, M. K. Hwang, A. Maffa, E. Balkanska-Sinclair, M. B. Yaffe, S. R. Floyd, P. T. Hammond, *Nat. Commun.* **2018**, *9*, 1991.
[5] M. Colin, C. Delporte, R. Janky, A. S. Lechon, G. Renard, P. Van Antwerpen, W. A. Maltese, V. Mathieu, *Cancers* **2019**, *11*, 411.
[6] J. J. Raizer, L. E. Abrey, A. B. Lassman, S. M. Chang, K. R. Lamborn, J. G. Kuhn, W. K. A. Yung, M. R. Gilbert, K. A. Aldape, P. Y. Wen, H. A. Fine, M. Mehta, L. M. DeAngelis, F. Lieberman, T. F. Cloughesy, H. I. Robins, J. Dancey, M. D. Prados, N. A. B. T. Consortium, *Neuro-Oncology* **2010**, *12*, 95.
[7] D. A. Reardon, J. A. Quinn, J. J. Vredenburgh, S. Gururangan, A. H. Friedman, A. Desjardins, S. Sathornsumetee, J. E. Herndon, J. M. Dowell, R. E. McLendon, J. M. Provenzale, J. H. Sampson, R. P. Smith, A. J. Swaisland, J. S. Ochs, P. Lyons, S. Tourt-Uhlig, D. D. Bigner, H. S. Friedman, J. N. Rich, *Clin. Cancer Res.* **2006**, *12*, 860.
[8] W. K. A. Yung, J. J. Vredenburgh, T. F. Cloughesy, P. Nghiemphu, B. Klencke, M. R. Gilbert, D. A. Reardon, M. D. Prados, *Neuro-Oncology* **2010**, *12*, 1061.
[9] K. Y. Y. Fung, G. D. Fairn, W. L. Lee, *Traffic* **2018**, *19*, 5.
[10] S. Lakkadwala, B. D. Rodrigues, C. W. Sun, J. Singh, *J. Controlled Release* **2019**, *307*, 247.
[11] D. G. Kim, M. S. Bynoe, *J. Clin. Invest.* **2016**, *126*, 1717.
[12] A. Shergalis, A. Bankhead, U. Luesakul, N. Muangsin, N. Neamati, *Pharmacol. Rev.* **2018**, *70*, 412.
[13] M. Touat, A. Idbaih, M. Sanson, K. L. Ligon, *Ann. Oncol.* **2017**, *28*, 1457.
[14] S. Sindhwani, A. M. Syed, J. Ngai, B. R. Kingston, L. Maiorino, J. Rothschild, P. MacMillan, Y. W. Zhang, N. U. Rajesh, T. Hoang, J. L. Y. Wu, S. Wilhelm, A. Zilman, S. Gadde, A. Sulaiman, B. Ouyang, Z. Lin, L. S. Wang, M. Egeblad, W. C. W. Chan, *Nat. Mater.* **2020**, *19*, 566.
[15] C. D. Arvanitis, G. B. Ferraro, R. K. Jain, *Nat. Rev. Cancer* **2020**, *20*, 26.
[16] W. A. Banks, *Nat. Rev. Drug Discovery* **2016**, *15*, 275.
[17] J. C. Ullman, A. Arguello, J. A. Getz, A. Bhalla, C. S. Mahon, J. H. Wang, T. Giese, C. Bedard, D. J. Kim, J. R. Blumenfeld, N. Liang, R. Ravi, A. A. Nugent, S. S. Davis, C. N. Ha, J. Duque, H. L. Tran, R. C. Wells, S. Lianoglou, V. M. Daryani, W. Kwan, H. Solanoy, H. Nguyen, T. Earr, J. C. Dugas, M. D. Tuck, J. L. Harvey, M. L. Reyzer, R. M. Caprioli, S. Hall, S. Poda, P. E. Sanchez, M. S. Dennis, K. Gunasekaran, A. Srivastava, T. Sandmann, K. R. Henne, R. G. Thorne, G. Di Paolo, G. Astarita, D. Diaz, A. P. Silverman, R. J. Watts, Z. K. Sweeney, M. S. Kariolis, A. G. Henry, *Sci. Transl. Med.* **2020**, *12*, eaay1163.
[18] M. S. Kariolis, R. C. Wells, J. A. Getz, W. Kwan, C. S. Mahon, R. Tong, J. Kim, A. Srivastava, C. Bedard, K. R. Henne, T. Giese, V. A. Assimon, X. C. Chen, Y. Zhang, H. Solanoy, K. Jenkins, P. E. Sanchez, L. Kane, T. Miyamoto, K. S. Chew, M. E. Pizzo, N. Liang, M. E. K. Calvert, S. L. DeVos, S. Baskaran, S. Hall, Z. K. Sweeney, R. G. Thorne, R. J. Watts, M. S. Dennis, A. P. Silverman, Y. J. Y. Zuchero, *Sci. Transl. Med.* **2020**, *12*, eaay1359.
[19] E. Aranda, C. Lopez-Pedrera, J. R. De La Haba-Rodriguez, A. Rodriguez-Ariza, *Curr. Mol. Med.* **2012**, *12*, 50.
[20] V. Somasundaram, D. Basudhar, G. Bharadwaj, J. H. No, L. A. Ridnour, R. Y. S. Cheng, M. Fujita, D. D. Thomas, S. K. Anderson, D. W. McVicar, D. A. Wink, *Antioxid. Redox Signaling* **2019**, *30*, 1124.
[21] C. Szabo, *Nat. Rev. Drug Discovery* **2016**, *15*, 185.
[22] S. Mocellin, V. Bronte, D. Nitti, *Med. Res. Rev.* **2007**, *27*, 317.
[23] J. Meng, Z. Y. Lv, Y. M. Zhang, Y. Y. Wang, X. H. Qiao, C. X. Sun, Y. Z. Chen, M. M. Guo, W. S. Han, A. J. Ye, T. Xie, B. Y. Chu, C. Shi, S. P. Yang, C. Chen, *Antioxid. Redox Signaling* **2020**, https://doi.org/10.1089/ars.2020.8212.
[24] X. Q. Wang, W. J. Wang, M. Y. Peng, X. Z. Zhang, *Biomaterials* **2021**, *266*, 120474.
[25] R. Chandrawati, J. Y. H. Chang, E. Reina-Torres, C. Jumeaux, J. M. Sherwood, W. D. Stamer, A. N. Zelikin, D. R. Overby, M. M. Stevens, *Adv. Mater.* **2017**, *29*, 1604932.
[26] A. W. Carpenter, M. H. Schoenfisch, *Chem. Soc. Rev.* **2012**, *41*, 3742.
[27] Y. C. Sung, P. R. Jin, L. A. Chu, F. F. Hsu, M. R. Wang, C. C. Chang, S. J. Chiou, J. T. Qiu, D. Y. Gao, C. C. Lin, Y. S. Chen, Y. C. Hsu, J. Wang, F. N. Wang, P. L. Yu, A. S. Chiang, A. Y. Wu, J. J. Ko, C. P. Lai, T. T. Lu, Y. Chen, *Nat. Nanotechnol.* **2019**, *14*, 1160.
[28] M. V. Simon, F. H. P. Spalm, L. E. Politi, N. P. Rotstein, *Invest. Ophthalmol. Visual Sci.* **2015**, *56*, 5808.
[29] N. J. Pyne, S. Pyne, *Nat. Rev. Cancer* **2010**, *10*, 489.
[30] M. Maceyka, S. Spiegel, *Nature* **2014**, *510*, 58.
[31] E. Bernhart, S. Damm, A. Wintersperger, C. Nusshold, A. M. Brunner, I. Plastira, G. Rechberger, H. Reicher, C. Wadsack, A. Zimmer, E. Malle, W. Sattler, *Biochem. Pharmacol.* **2015**, *96*, 119.
[32] A. Weyerbrock, N. Osterberg, N. Psarras, B. Baumer, E. Kogias, A. Werres, S. Bette, J. E. Saavedra, L. K. Keefer, A. Papazoglou, *Neurosurgery* **2012**, *70*, 497.
[33] E. Baltruskeviciene, B. Kazbariene, R. Badaras, L. Bagdonaite, A. Krikstaponiene, L. Zdanavicius, E. Aleknavicius, J. Didziapetriene, *Turk. J. Gastroenterol.* **2016**, *27*, 336.
[34] S. Tsuchida, Y. Sekine, R. Shineha, T. Nishihira, K. Sato, *Cancer Res.* **1989**, *49*, 5225.
[35] H. Kojima, Y. Urano, K. Kikuchi, T. Higuchi, Y. Hirata, T. Nagano, *Angew. Chem., Int. Ed.* **1999**, *38*, 3209.
[36] Q. Zhou, S. Shao, J. Wang, C. Xu, J. Xiang, Y. Piao, Z. Zhou, Q. Yu, J. Tang, X. Liu, Z. Gan, R. Mo, Z. Gu, Y. Shen, *Nat. Nanotechnol.* **2019**, *14*, 799.
[37] T. E. Park, N. Mustafaoglu, A. Herland, R. Hasselkus, R. Mannix, E. A. FitzGerald, R. Prantil-Baun, A. Watters, O. Henry, M. Benz, H. Sanchez, H. J. McCrea, L. C. Goumnerova, H. W. Song, S. P. Palecek, E. Shusta, D. E. Ingber, *Nat. Commun.* **2019**, *10*, 2621.
[38] K. P. Locher, *Nat. Struct. Mol. Biol.* **2016**, *23*, 487.
[39] S. Kunjachan, B. Rychlik, G. Storm, F. Kiessling, T. Lammers, *Adv. Drug Delivery Rev.* **2013**, *65*, 1852.
[40] L. Riboni, L. A. Hadi, S. E. Navone, L. Guarnaccia, R. Campanella, G. Marfia, *Cells* **2020**, *9*, 337.

[41] A. Cartier, T. Hla, *Science* **2019**, *366*, eaar5551.
[42] R. E. Cannon, J. C. Peart, B. T. Hawkins, C. R. Campos, D. S. Miller, *Proc. Natl. Acad. Sci. USA* **2012**, *109*, 15930.
[43] P. Chongsathidkiet, C. Jackson, S. Koyama, F. Loebel, X. Cui, S. H. Farber, K. Woroniecka, A. A. Elsamadicy, C. A. Dechant, H. R. Kemeny, L. Sanchez-Perez, T. A. Cheema, N. C. Souders, J. E. Herndon, J. V. Coumans, J. I. Everitt, B. V. Nahed, J. H. Sampson, M. D. Gunn, R. L. Martuza, G. Dranoff, W. T. Curry, P. E. Fecci, *Nat. Med.* **2018**, *24*, 1459.
[44] B. Ogretmen, *Nat. Rev. Cancer* **2018**, *18*, 33.
[45] L. Hasanifard, R. Sheervalilou, M. Majidinia, B. Yousefi, *J. Cell. Physiol.* **2019**, *234*, 8162.
[46] A. Weyerbrock, N. Osterberg, N. Psarras, B. Baumer, E. Kogias, A. Werres, S. Bette, J. E. Saavedra, L. K. Keefer, A. Papazoglou, *Neurosurgery* **2012**, *70*, 497.
[47] J. Guenzle, N. W. C. Garrelfs, J. M. Goeldner, A. Weyerbrock, *Mol. Neurobiol.* **2019**, *56*, 6046.
[48] G. Tan, A. Wu, Z. Li, P. Awasthi, *Transl. Cancer Res.* **2019**, *8*, 1602.